18

New upconversion bulk and nanophosphors based on the $Sr_2Y_{8-x-y}Yb_yTm_xSi_6O_{26}$

© M.G. Zuev[1], A.A. Vasin[1], V.G. Ilves[2], S.Yu. Sokovnin[2,3]

[1] Institute of Solid State Chemistry, Russian Academy of Sciences, Ural Branch, Yekaterinburg, Russia
[2] Institute of Electrophysics, Ural Branch, Russian Academy of Sciences, Yekaterinburg, Russia
[3] Ural Federal University after the first President of Russia B.N. Yeltsin, Yekaterinburg, Russia; Institute of Electrophysics, Ural Branch, Russian Academy of Sciences, Yekaterinburg, Russia

e-mail: zuev@ihim.uran.ru

Received October 14, 2022
Revised November 07, 2022
Accepted November 24, 2022

Polycrystalline phosphors with a $Sr_2Y_{8-x-y}Yb_yTm_xSi_6O_{26}$ ($x = 0.005-0.5$, $y = 0.2, 0.3$) total formula were synthesized. Nanoluminophor has been obtained from the $Sr_2Y_{7.695}Yb_{0.3}Tm_{0.005}Si_6O_{26}$ microcrystalline sample by the vacuum electron been evaporation, in the amorphous state, with the ~ 10.6 nm particle size. It is found, raman spectra undergoing modification by the transition from bulk- to nanosize state. Photoluminescene spectra micro- and nanophosphors are studied. Intensity of the blue emission, by the UV ligth excitation, grows in the $x = 0.005-0.02$ region, with the x increasing. Upconversion photoluminescence (UPCL) spectra of the bulk phosphors and nanosample based on the $Sr_2Y_{7.695}Yb_{0.3}Tm_{0.005}Si_6O_{26}$ were measurd. At the pumping power around 70.8 mW, by the laser source with the $\lambda = 980$ nm, thereshold population of the $^3F_3$ level of Tm^{3+} ions exist. At a power higher 70.8 mW, a sharp increase of the luminescence intensityof the bulk- and nanophosphor occurs. For the $^3H_4 \rightarrow {}^3H_6$ transition thereshold pumping power absent. This indicates that, pumping, during Yb→Tm energy transer, is a single photon process.

Keywords: Photoluminescence, Tm^{3+}, Yb^{3+} ions, raman spectra.

DOI: 10.61011/EOS.2023.05.56517.55-22

Introduction

The search for new phosphors for use in various fields of technology and medicine is of great scientific and practical importance. In particular, the synthesis and study of the characteristics of upconversion phosphors attracts attention and is widely discussed by researchers [1]. Upconversion phosphors are used in displays and in bioimaging due to the fact that infrared (IR) light does not affect biological tissues [2]. They are also used in other areas [3]. Silicate phosphors containing rare earth elements (REE) are known as effective compounds with high-intensity luminescence in the visible spectrum, promising, for example, for designing LED devices. For example, silicates with an apatite structure are known as effective matrices for their activation by REE ions. These materials can be used as active laser media and phosphors [4–7] due to the high luminescence intensity and chemical stability up to 1000°C. Reduction of phosphor particles from micro- to nanosize leads to the appearance of spectral-luminescent characteristics that differ from those for bulk samples. It has been shown in some papers that the intensity of the luminescence of REE ions is higher in amorphous nanoluminophores than in bulk samples [8,9]. Nanophosphors allow to design new phosphors, as well as multifunctional devices, for example, for luminescent visualization of measurements of thermodynamic, mechanical and other parameters in various systems [10].

Nanoparticles are obtained by various methods. There are dispersion, condensation, gas, liquid, solid phase and other methods. Nanophosphors are often synthesized using sol-gel processes, resulting in core-shell structures [3]. The monograph [11] describes in detail a new method for obtaining oxide nanoparticles based on the evaporation-condensation process using a pulsed electron beam (PEB). Samples are obtained by evaporation of ceramic targets in vacuum using a PEB. The method allows to obtain chemically pure samples. The applied electron beam allows to reduce some activator ions in the phosphor matrix and thereby change the spectral characteristics of the samples.

As an example, one can point to the work [12], in which new nanoluminophores were obtained by the PEB method by electron beam evaporation in a vacuum or an argon atmosphere of germanates of the composition $Ca_2La_8(GeO_4)_6O_2:E$ The reduction of $Eu^{3+} \rightarrow Eu^{2+}$ ions in an electron beam was found.

It is of interest to study the dependence of the characteristics of upconversion photoluminescence (UCPL) of bulk and nanoluminophores on the method of their preparation, to study the effect of the transition from bulk to nano-sized luminophores on the spectral composition of UCPL. In particular, it is important to study the dependence of energy transfer processes on the power of pumping samples

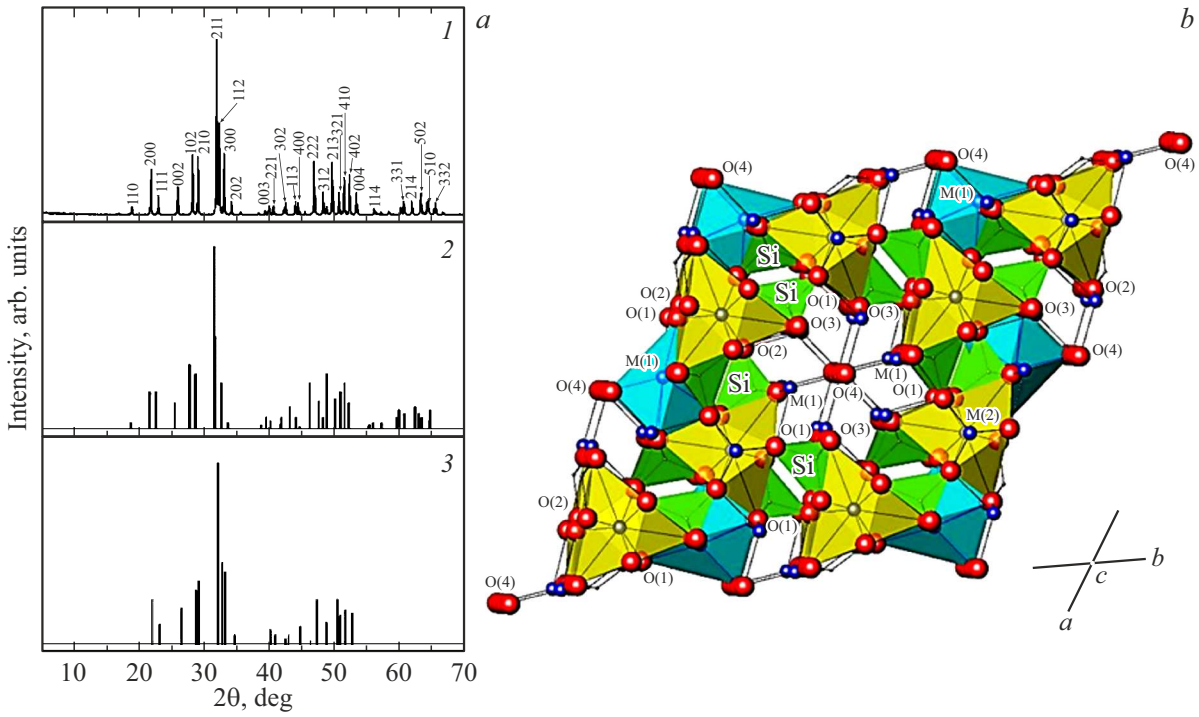

Figure 1. (*a*) Diffraction patterns: $Sr_2Y_{7.695}Yb_{0.3}Tm_{0.005}(SiO_4)_6O_2$ (*1*), $Sr_2Eu_8(SiO_4)_6O_2$ (*2*), $Y_{9.33}(SiO_4)_6O_2$ (*3*). (*b*) Structure of solid solutions $Sr_2Y_{8-x-y}Yb_yTm_x(SiO_4)_6O_2$.

with laser radiation. It is of interest to determine the type of energy transfer processes for relatively low pumping powers.

Research objectives: to synthesize polycrystalline silicates of the composition $Sr_2Y_{8-x-y}Yb_yTm_xSi_6O_{26}$, to obtain nanoluminophores based on bulk samples using the IEP method, to analyze the Raman spectra (RS) of micro- and nanosamples, to determine some spectral-luminescent characteristics of phosphors, to study the dependences of the intensity logarithm I UCPL of samples from the logarithm of power P of pumping by a laser with a power of less than 220 mW and a wavelength of 980 nm.

The purpose of this study: to develop methods for the synthesis of new oxide silicate bulk and nanoluminophores containing thulium and ytterbium ions, and to determine the spectral and luminescent characteristics of the synthesized samples; to consider the processes of UCPL of phosphors during the transition from micro- to nano-sized phosphors obtained by the BEP method.

The developed new methods for the production of phosphors and the results of studying their spectral and luminescent characteristics will allow to outline ways of creating new oxide optical materials.

Materials and methods

Polycrystalline samples of the composition $Sr_2Y_{8-x-y}Yb_yTm_xSi_6O_{26}$ ($x = 0.005-0.5$, $y = 0.2, 0.3$) were obtained by the sol-gel synthesis method similar to that described in the papers [13–15]. The choice of concentrations of Yb and Tm ions is due to the achievement of the highest intensity of UCPL excited in the near-IR range [16]. Initial components Y_2O_3, $SrCO_3$, Yb_2O_3, Tm_2O_3 were dissolved in nitric acid. The oxide SiO_2 was triturated with citric acid. A solution of nitrates was added to the resulting gel, then a solution of citric acid in ethanol was added. The resulting white precipitate was calcined at 1400°C for 30 h.

The completeness of the synthesis was checked by X-ray diffraction analysis (XRDA) using a Shimadzu XRD-7000 diffractometer (CuK_α radiation). Scanning was carried out at room temperature. The diffraction patterns of the obtained samples, recorded in the angle range $2\theta = 5-70°$, were processed by the Rietveld method.

The UCPL spectra were recorded on an MDR-204 spectrometer (deuterium lamp, KLM-H980-200-5, PMT R928 laser module, Hamamatsu). Stokes photoluminescence and excitation spectra were recorded in the accumulation mode on an Edinburg Instruments FS5 spectrofluorimeter equipped with a 450 W ozone-free Xe lamp and a Hamamatsu R928P photomultiplier for measurements in the 200–900 nm wavelength range. The spectral resolution ±0.5 nm. The Raman spectra were recorded on a Renishaw inVia Qontor confocal Raman microscope using a laser ($\lambda = 785$ nm) with an installed power of 3 mW and a resolution of 0.3 cm^{-1}.

Nanopowders (NP) were obtained by evaporation of ceramic targets in the form of pellets pressed from powders

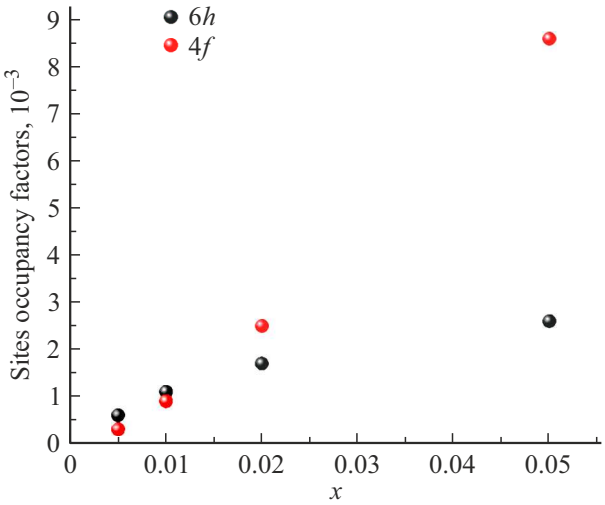

Figure 2. Dependence of the occupation of cationic positions by Tm^{3+} ions in samples $Sr_2Y_{8-x-y}Yb_yTm_x(SiO_4)_6O_2$.

of polycrystalline samples. Diameter of tablets 20 mm, thickness — 16.5 mm. Tablets before evaporation were calcined at a temperature of 1200°C for 40 h. Evaporation was carried out in vacuum using an PEB on a NANOBIM-2 [11] unit. The electron energy was 40 keV, the electron beam pulse energy was 1.8 J, and the pulse frequency was 20–50 Hz. Target evaporation time — 40 min. Nanopowders were deposited on uncooled glass substrates placed around the target. The specific surface area of the powders (S_{sp}) was determined by the Brunauer–Emmett–Taylor (BET)[13] [17] method on a Micromeritics TriStar3000 unit. Microscopic analysis of NP was performed on a JEOLJEM 2100 transmission electron microscope.

Results and discussion

Bulk samples

Fig. 1, *a* shows a characteristic diffraction pattern of the synthesized solid solution. It has been specified that, during crystallization, these compositions form an apatite-type phase (sp. gr. $P6_3/m$). To indicate reflexes on the diffraction patterns, ICDD files were used: crystals $Sr_2Eu_8(SiO_4)_6O_2$ (card 00-029-1300) and $Y_{9.33}(SiO_4)_6O_2$ (Card 00-030-1457).

The structure of the presented compounds (Fig. 1, *b*) is characterized by the presence of two nonequivalent cationic positions. Positions M(1) (6*h*), which are occupied by ions Sr^{2+}, Y^{3+}, Yb^{3+}, Tm^{3+}, are located inside the polyhedra M(1) O_7. In Fig. 1, *b* the polyhedra M(1) O_7 are presented as blue disphenoids. The positions M(2) (4*f*) are located inside the polyhedra M(2) O_9 (shown in yellow).

The O(1), O(2) and O(3) ions together with the Si^{4+} ions, are located in 6*h* positions, form tetrahedral anionic groups $[SiO_4]^{4-}$ (shown in green in Fig. 1, *b*). Ions O(4) are located in the channels *2a* and form bonds M(1)–O(4). The results of calculation of crystal chemical parameters are presented in the table. The values of uncertainty factors — experimental $R_{exp}(\%)$ and profile $R_p(\%)$ — and quality criterion of structure refinement χ^2 are also indicated here.

In Fig. 2 there is dependence of the occupation of cationic positions by Tm^{3+} ions in samples $Sr_2Y_{8-x-y}Yb_yTm_x(SiO_4)_6O_2$. It can be seen from Fig. 2 that with an increase in the concentration of x, the occupation of positions M(2) by thulium ions increases. In the paper [18], the process of substitution of Y^{3+} ions for Eu^{3+} ions in solid solutions of $Sr_2Y_{8-x}Eu_x(SiO_4)_6O_2$) was reviewed and uneven filling of cationic positions was also noted, at which 4*f* — channels began to fill with europium at $x > 0.02$. Effective ionic radii $r_{Sr^{2+}} = 1.21$ Å (coordination number CN=7), $r_{Sr^{2+}} = 1.31$ Å (CN=9), $r_{Y^{3+}} = 0.96$ Å (CN=7), $r_{Y^{3+}} = 1.08$ Å (CN=9), $r_{Tm^{3+}} = 0.93$ Å (CN=7), $r_{Tm^{3+}} = 1.05$ Å (CN=9), $r_{Yb^{3+}} = 0.93$ Å (CN=7), $r_{Yb^{3+}} = 1.04$ Å (CN=9) [19]. Since the ionic radii Yb^{3+} and Tm^{3+} are closer to the ionic radius Y^{3+}, then the position for which the ratio of the content of Y^{3+}/Sr^{2+} ions is greater is i. e. 6*h*. An increase in the content of Yb^{3+} and Tm^{3+} in 4*f* positions leads to an increase in cation vacancies for samples with $x = 0.02$ and $x = 0.05$ The proposed mechanism for the formation of such vacancies:

$$3Sr_{Sr}^{\times} + 2REE^{\bullet\bullet\bullet} \rightarrow 2REE_{Sr}^{\bullet} + V_{Sr}'' + 3Sr^{\bullet\bullet},$$

where $REE = Yb^{3+}$, Tm^{3+}.

Stokes luminescence of samples $Sr_2Y_{8-x-y}Yb_yTm_x(SiO_4)_6O_2$

Photoluminescence was excited by radiation with $\lambda_{ex} = 358$ nm corresponding to the $^3H_6 \rightarrow {}^1D_2$ transition (Fig. 3, *a*). In the 430–700 nm area, a series of narrow lines (Fig. 3, *b*) corresponding to $f-f$-transitions of the Tm^{3+} ion was registered. The most intense is the line with a peak at 458 nm, corresponding to the transition $^1D_2 \rightarrow {}^3F_4$ [20]. For samples with $x = 0.005$ and 0.01, a series of intense lines also appear in the red area, corresponding to the transitions $^1G_4 \rightarrow {}^3F_4$ (636 nm), $^3F_2 \rightarrow {}^3H_6$ (660 nm), $^1D_2 \rightarrow {}^3H_4$ (674 nm) [21]. Also in the green area there is a line with a peak at 519 nm, corresponding to the transition $^1D_2 \rightarrow {}^3H_5$ [20]. The transition $^1G_4 \rightarrow {}^3H_6$ (474 nm) is also registered. For compounds with $x = 0.02$ and $x = 0.05$ in the near-IR area, there are two intense lines at 758 and 790 nm, corresponding to the transitions $^1G_4 \rightarrow {}^3H_5$ and $^3H_4 \rightarrow {}^3H_6$ [22,23], and for samples with a lower concentration of thulium, the intensity of these lines is lower. But for the sample with $x = 0.05$ the intensity of the lines in the area of 500–700 nm is lower than in the samples with a lower content of Tm^{3+}. In addition, the samples with $x = 0.005$ and $x = 0.01$ contain lines corresponding to transitions from higher excited states than $^1D_2$, in particular, $^3P_2 \rightarrow {}^1G_4$ (604 nm), $^3P_0 \rightarrow {}^3F_2$ (555 nm). This feature of the samples can be explained by the high population of

Crystal chemical parameters of the samples $Sr_2Y_{8-x-y}Yb_yTm_x(SiO_4)$

Parameters	Samples					
	$x = 0.005, y = 0.2$	$x = 0.005, y = 0.3$	$x = 0.01, y = 0.2$	$x = 0.01, y = 0.3$	$x = 0.02, y = 0.3$	$x = 0.05, y = 0.3$
a, Å	9.3625	9.3926	9.3672	9.3998	9.3940	9.4009
c, Å	6.8571	6.8646	6.8666	6.8620	6.8581	6.8898
a/c	1.3654	1.3683	1.3642	1.3698	1.3698	1.3645
V, Å^3	520.544	524.470	521.789	525.075	524.129	527.326
R_{exp}, %	16.25	13.55	14.32	13.05	12.91	12.58
R_p, %	15.2	14.2	14.3	15.1	13.3	14.7
χ^2	1.47	1.79	1.65	2.26	1.73	2.25

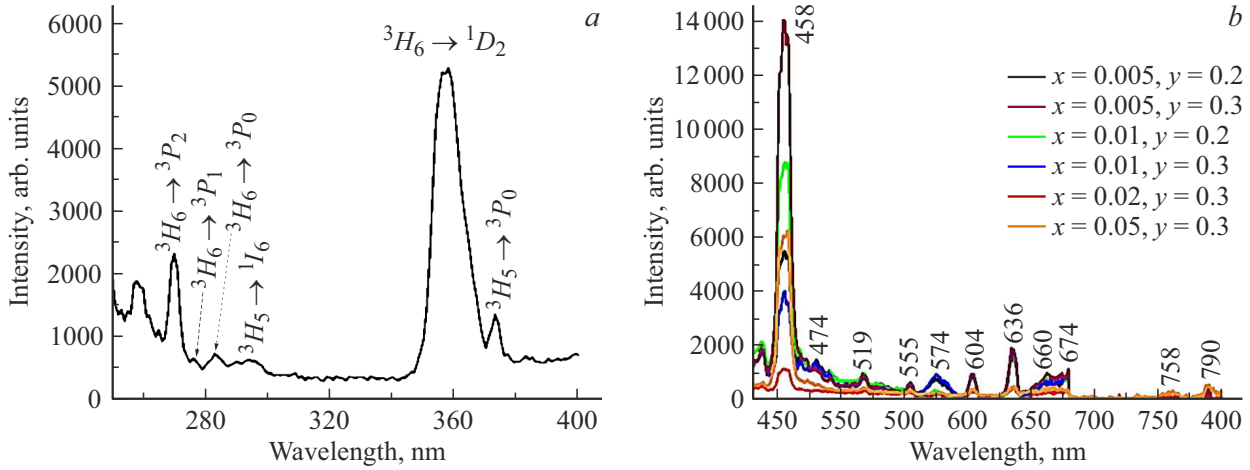

Figure 3. (a) Excitation spectrum ($\lambda_{em} = 458$ nm) of the sample $Sr_2Y_{7.65}Yb_{0.3}Tm_{0.05}(SiO_4)_6O_2$. ($b$) Photoluminescence spectra of the samples $Sr_2Y_{8-x-y}Yb_yTm_x(SiO_4)_6O_2$.

the $^3F_4$, $^3H_5$ and $^3H_4$ levels. Since at a low concentration of Tm^{3+} the intensity of the multipole-multipole interaction turns out to be low, the probability of the $^1G_4 \rightarrow {}^3F_4$, $^1D_2 \rightarrow {}^3H_4$, $^1D_2 \rightarrow {}^3H_5$ transitions increases, which leads to an increase in the intensity of the corresponding lines. In addition, the probability of interaction between the $4f^{12}$-shell of the Tm^{3+} ion and the phonons of matrix vibrations increases. Thus, a broad line with a peak at 574 nm can be described in terms of the relaxation of a metastable state ($^1D_2 + \hbar\omega_{host}$) into a state $^3H_4$. The intensity of the line corresponding to the $^1D_2 \rightarrow {}^3F_4$ transition increases in the concentration range of thulium ions from 0.005 to 0.02. Thus, the exciting radiation is absorbed by thulium ions not only in the $^3H_6$ state, but also in states at higher energy levels. In this case, the intensity of emission during relaxation of electrons from the states $^3F_4$, $^3H_5$, $^3H_4$ to the ground state for samples with a lower content of Tm^{3+} turns out to be lower.

The maximum integrated luminescence intensity of the $Sr_2Y_{8-x-y}Yb_yTm_x(SiO_4)_6O_2$) solid solutions is noted for the composition with $x = 0.02$ and 0.3, i.e., for the composition with an almost equal content of Tm^{3+} ions in two cationic positions.

Nanoscale samples

A sample of $Sr_2Y_{7.695}Yb_{0.3}Tm_{0.005}Si_6O_{26}$ with the highest Tm^{3+} ion luminescence intensity was chosen to obtain a nanosample. Fig. 4, a shows the particles of the obtained nanosample. On the electron diffraction pattern of the nanoparticles (Fig. 4, b) strongly blurred diffuse rings which indicate the amorphous nature of the sample can be seen. The BET value of the surface of the $S_{sp} = 118.7768\ m^2/g$ nanopowder. Therefore, the average particle size is ~ 10.6 nm.

Fig. 5 shows the Raman spectra of bulk and nanosized phosphors of the composition $Sr_2Y_{7.695}Yb_{0.3}Tm_{0.005}(SiO_4)_6O_2$. The difference between a nanosample and a bulk sample is that, in addition to the vibrational frequencies of isolated [SiO_4] tetrahedra, the spectrum contains frequencies corresponding to the vibrations of Si−O−Si groups, in which the tetrahedra are

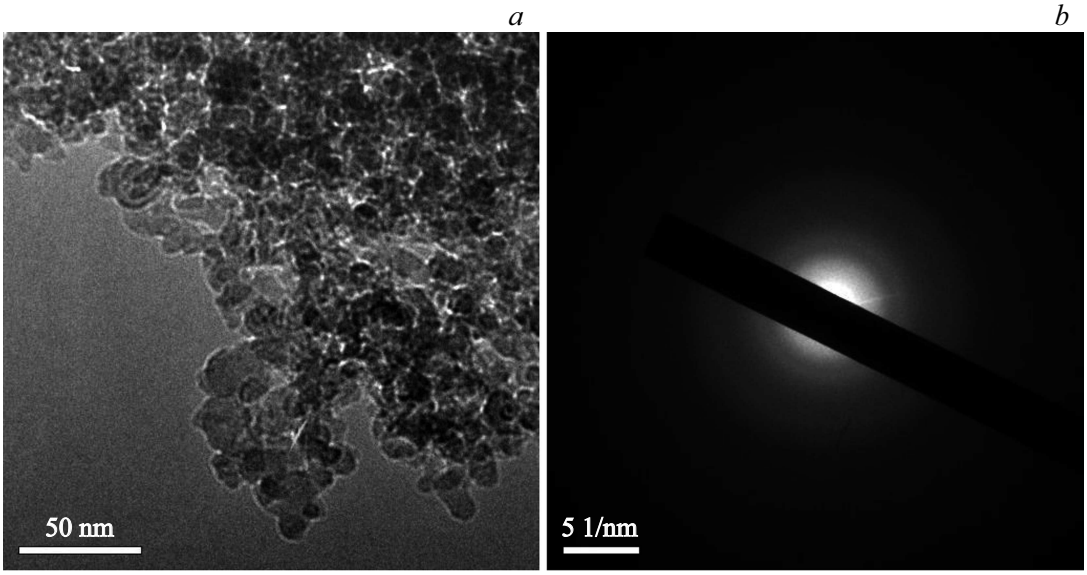

Figure 4. (*a*) TEM HR image and (*b*) IR electron diffraction pattern based on $Sr_2Y_{7.695}Yb_{0.3}Tm_{0.005}Si_6O_{26}$.

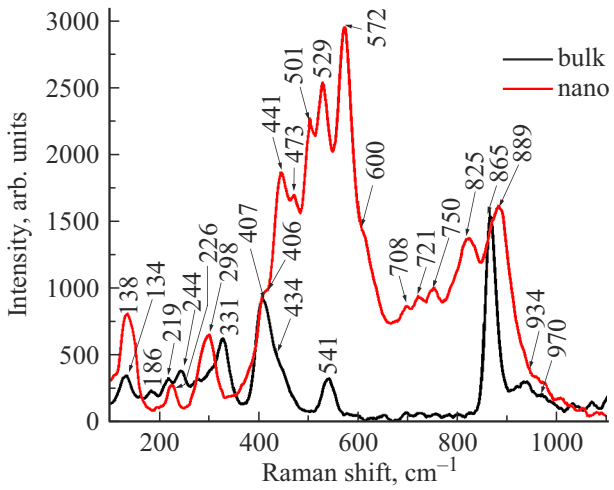

Figure 5. Spectra of the bulk sample and nanopowder of the compound $Sr_2Y_{7.695}Yb_{0.3}Tm_{0.005}(SiO_4)_6O_2$.

connected via „bridging" ions O^{2-}. In the 440–600 cm^{-1} area, oscillations corresponding to ring structures are identified, and in the 600–770 cm^{-1} area — to chain [22] structures. The presence of these lines indicates the polymerization of silicon–oxygen groups during the formation of a nanoamorphous state. This phenomenon can be explained by the peculiarities of the preparation method: the breaking of Si–O bonds during the evaporation of a bulk sample by an electron beam is accompanied by the formation of defective tetrahedra $[SiE'O_3V_O^{\bullet}]$ and linear $SiE''O_2V_{O^2}^{\bullet}$ radicals, where E' and E'' are one- and two-electron centers on silicon. During condensation on a substrate, grain growth is accompanied by the interaction of SiO_4 defects with the formation of chain and ring clusters. The shift in the frequency of symmetric stretching vibrations to the high-frequency region (889 cm^{-1}) indicates a reduction in the Si–O bond length.

Let us review the UCPL spectra of bulk samples and nanosamples (Fig. 6). The UCPL spectra were recorded upon excitation by IR laser radiation ($\lambda = 980$ nm) at different powers P of laser radiation.

For a nanosample, as the pump power decreases from 220 to 177 mW, the half-width of the transition lines $^3H_4 \rightarrow {}^3H_6$ decreases significantly (Fig. 6, *b*). This is probably due to the difference in the populations of the corresponding levels for bulk and nanosamples.

Fig. 7 shows the dependences of the logarithm of the UCPL intensity on the logarithm of the pumping power for some transitions of the Tm^{3+} ion.

The lines on the graphs are drawn with an error of 2.5% for each value of $\ln I$. There is a characteristic value of the threshold power for the transition $^3F_3 \rightarrow {}^3H_6$ at $P \sim 70.8$ mW. In power interval 20–70.8 mW, the slope of the dependence line is close to 0.2 (Fig. 7, *a*), probably due to the small effect of the pump power on the population of the $^3F_3$ level. At a power above 70.8 mW, a sharp increase in the UCPL intensity occurs. The slope becomes close to 1. This means that the red UCPL is a two-photon process [24], which occurs according to the following diagram. The first photon from the $^2F_{5/2}$ state of the Yb^{3+} ion excites the $^3H_4$ state of the Tm^{3+} ion, the second photon excites the $^3H_5$ state of the Tm^{3+} ion with subsequent relaxation to the $^3F_4$ state. Then the $^3F_3$ state is excited. For the $^3H_4 \rightarrow {}^3H_6$ transition, the slope is close to 0.6 and there is no threshold pumping power. This indicates a single-photon pumping process during energy transfer Yb–Tm, in which a photon from the $^2F_{5/2}$ state of the Yb^{3+} ion excites the $^3H_4$ state of the Tm^{3+} ion with further relaxation to the $^3H_6$ state. For a

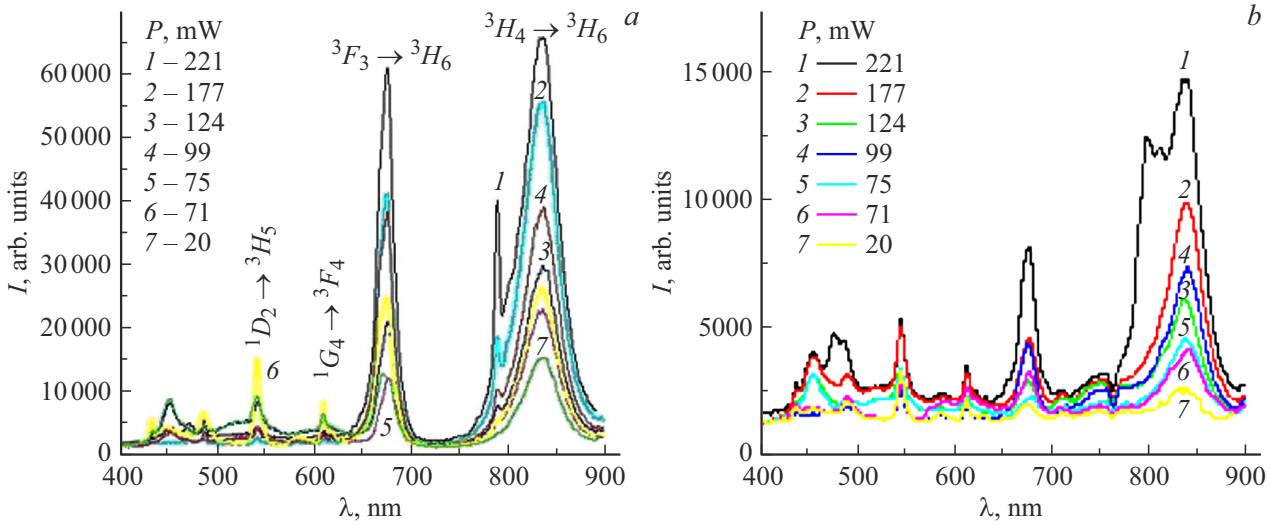

Figure 6. UCPL spectra of bulk samples (*a*) and nanosamples (*b*).

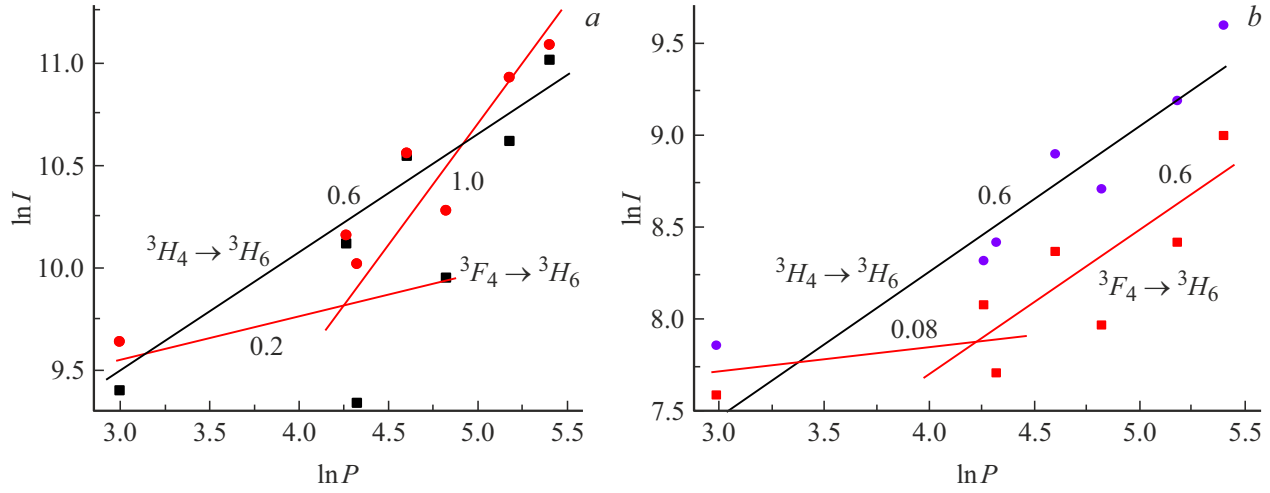

Figure 7. Dependences of the UCPL intensity on the pump power for $^3H_4 \rightarrow {}^3H_6$ (black and purple dots) and $^3F_3 \rightarrow {}^3H_6$ (red dots) transitions in bulk (*a*) and nanophosphors (*b*).

nanosample, there is the same threshold pumping power as for a bulk sample (Fig. 7, *b*).

The mechanisms of stokes luminescence and upconversion for $Sr_2Y_{8-x-y}Yb_yTm_x(SiO_4)_6O_2$) samples are presented in Fig. 8 (wavy arrows denote nonradiative transitions).

Conclusion

A method has been developed for obtaining new nanoluminophores by electron beam evaporation in vacuum of polycrystalline samples of the composition $Sr_2Y_{8-x-y}Yb_yTm_xSi_6O_{26}$ ($x = 0.005-0.5$, $y = 0.2, 0.3$). A modification of the Raman spectra was found when sample particles are reduced from the bulk to the nanoscale state. It has been established that during the preparation of nanoparticles through the evaporation of bulk samples, polymerization of $[SiO_4]$ tetrahedra occurs. Under UV excitation of bulk samples, the intensity of the blue emission in the $x = 0.005-0.02$ area increases with increasing x. The UCPL spectra of bulk phosphors and a nanosample based on $r_2Y_{7.695}Yb_{0.3}Tm_{0.005}Si_6O_{26}$ were studied. In the 70.8 mW area of phosphor pumping power by laser radiation with $\lambda = 980$ nm, there is a threshold population of the level $^3F_3$ of the Tm^{3+} ion. At a power above 70.8 mW, a sharp increase in the intensity of the luminescence of micro- and nanophosphorus occurs. For the $^3H_4 \rightarrow {}^3H_6$ transition there is no threshold pumping power. In comparison with the well-known upconversion nanoluminophore $NaLuF_4$ used in bioapplications: 24% Gd, 20% Yb, 2% Tm [25] the quantum efficiency increases by ~ 3 times in the proposed phosphors.

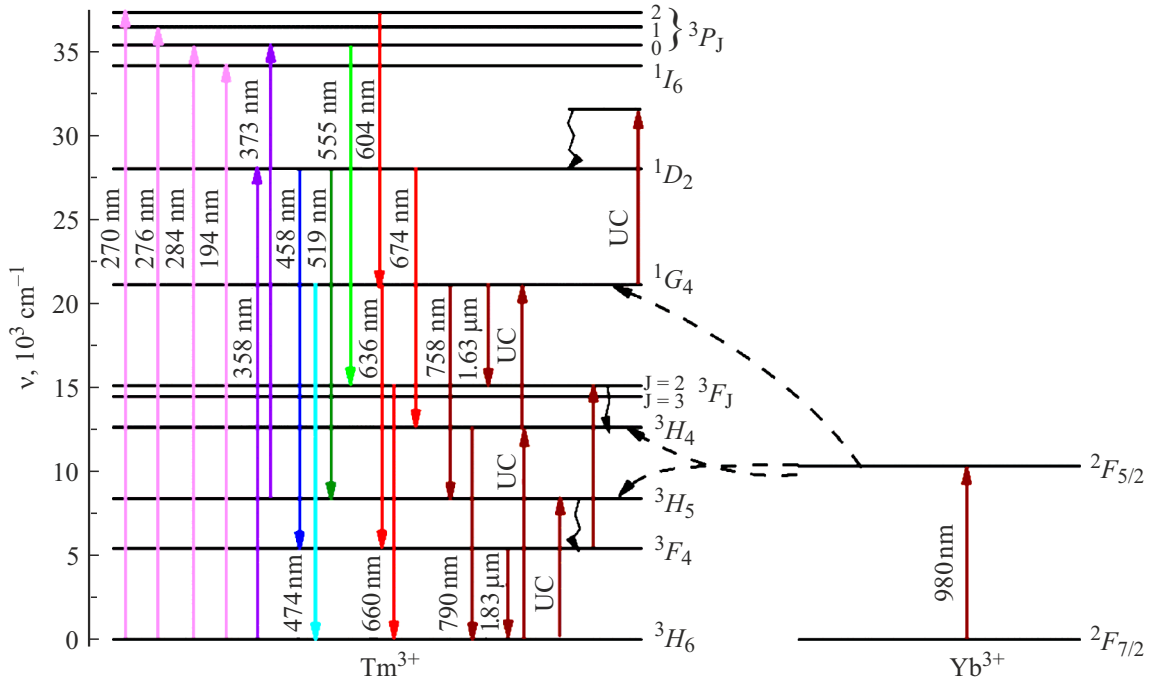

Figure 8. Mechanisms of luminescence under UV excitation and UCPL for Samples $Sr_2Y_{8-x-y}Yb_yTm_x(SiO_4)_6O_2$.

Conclusions

Abstract New upconversion bulk phosphors of the composition $Sr_2Y_{8-x-y}Yb_yTm_xSi_6O_{26}$ ($x = 0.005-0.5$, $y = 0.2, 0.3$) and a nanophosphor based on the $Sr_2Y_{7.695}Yb_{0.3}Tm_{0.005}Si_6O_{26}$. For the $^3F_3 \rightarrow {}^3H_6$ transition of the Tm^{3+} ion, a threshold pumping power of 70.8 mW was found, which is due to a sharp change in the population of the $^3F_3$ level. At a power above this value, a two-photon process of energy transfer Yb −Tm. occurs. At the same time, for the $^3H_4 \rightarrow {}^3H_6$ transition, there is a continuous change in the population of the $^3H_4$ level, which indicates a single-photon energy transfer process Yb−Tm.

Funding

The paper was carried out in accordance with the state assignment of the Institute of Solid State Chemistry, Ural Branch of the Russian Academy of Sciences and plans for research and development and was partially supported by the Russian Science Foundation, grant № 22-19-00239.

Conflict of interest

The authors declare that they have no conflict of interest.

References

[1] *Phosphors, Up Conversion Nano Particles, Quantum Dots and Their Applications* (Springer-Verlag, Berlin-Heidelberg, 2017). V. 2.

[2] B.J. Park, A-R. Hong, S. Park, K.-U. Kyung, K. Lee, H.S.Jang. Sci. Rep., 745659 (1917). DOI: 10.1038/srep45659

[3] F. Wang, R. Deng, J. Wang, Q. Wang, Y. Han, H. Zhu, X. Chen, X. Liu. Nature Materials, **10**, 968 (2011). DOI: 10.1038/nmat3149

[4] N.M. Khaidukov, M. Kirm, E. Feldbach, H. Magi, V. Nagirnyi, E. Toldsepp, S. Vielhauer, T. Jüstel, T. Jansen, V.N. Makhov. J. Lumin., **191**, 51 (2017). DOI: 10.1016/j.jlumin.2017.01.033

[5] T. Jansen, T. Jüstel, M. Kirm, H. Magi, V. Nagirnyi, E. Toldsepp, S. Vielhauer, N.M. Khaidukov, V.N. Makhov. J. Lumin., **186**, 205 (2017). DOI: 10.1016/j.jlumin.2017.02.004

[6] A.A. Vasin, M.G. Zuev, I.D. Popov, I.V. Baklanova, D.G. Kellerman, E.V. Zabolotskaya, Ju.G. Zajnulin, N.I. Kadyrova. Russ. J. Phys. Chem. A, **94**, 2467 (2020). DOI: 10.1134/S0036024420120316

[7] A.A. Vasin, M.G. Zuev, E.V. Zabolotskaya, I.V. Baklanova, L.A. Akashev, R.F. Sammigulina. J. Lumin., **169**, 26 (2015). DOI: 10.1016/j.jlumin.2015.07.019

[8] M.G. Zuev, S.Yu. Sokovnin, V.G. Il'ves, I.V. Baklanova, A.A. Vasin. J. Sol. State Chem., **218**, 164 (2014). DOI: 10.1016/j.jssc.2014.06.034

[9] M.G. Zuev, V.G. Il'ves, S.Yu. Sokovnin, A.A. Vasin. Results in Optics, **5**, 100189 (2021). DOI: 10.1016/j.rio.2021.100189

[10] C.C. Lin, R.-S. Liu. Introduction to the Basic Properties of Luminescent Materials (*in Phosphors, Up Conversion Nano Particles, QuantumDots and Their Applications*) (Springer, Berlin-Heidelberg, 2017). V. 1. DOI: https://doi.org/10.1007/978-3-662-52771-9

[11] S.Yu. Sokovnin, V.G. Il'ves, M.G. Zuev. *Engineering of Nanobiomaterials Applications of Nanobiomaterials* (Elsevier, Amsterdam, 2016). V. 2. Ch. 2.

[12] M.G. Zuev, V.G. Il'ves, S.Yu. Sokovnin, A.A. Vasin, I.V. Baklanova. Phys. Sol. St., **61** (5), 925 (2019). DOI: 10.1007/s11172-020-2854-z

[13] H. Gong, D.-Y. Tang, H. Huang, M.-D. Han, T. Sun, J. Zhang, X. Qin, J. Ma. J. Crystal Growth, **362** (1), 52 (2013). DOI: 10.1016/j.jcrysgro.2011.12.087
[14] D. Kioupis, G. Kakali. Ceram. Int., **42**, 9640 (2016). DOI: 10.1016/j.ceramint.2016.03.050
[15] V.A. Pustovarov, A.A. Vasin, M.G. Zuev. Opt. Mat., **15**, 100186 (2022). DOI: 10.1016/j.omx.2022.100186
[16] C. Alarcón-Fernández, C. Zaldo, C. Cascales. J. All. Comp., **913**, 165180 (2022). DOI: 10.1016/j.jallcom.2022.165180
[17] S. Brunauer. *Adsorbtsiya gazov i parov. Fizicheskaya adsorbtsiya.* (GIIL, M., 1948) (in Russian). T. 1.
[18] M.G. Zuev, A.M. Karpov, A.S. Shkvarin. J. Sol. St. Chem., **184**, 52 (2011). DOI: 10.1016/j.jssc.2010.10.014
[19] R.D. Shannon. Acta Cryst., **A32**, 751 (1976). DOI: 10.1107/S0567739476001551
[20] A. Jusza, L. Lipińska, M. Baran, P. Polis, A. Olszyna, R. Piramidowicz. Opt. Mat., **971**, 09365 (2019). DOI: 10.1016/j.optmat.2019.109365
[21] K. Janani, S. Ramasubramanian, P. Thiyagarajan. Materials Today: Proceedings, **33** (5), 2082 (2020). DOI: 10.1016/j.matpr.2020.02.091
[22] L. Xu, C. Xu. Ceram. Int., **46**, 19425 (2020). DOI: 10.1016/j.ceramint.2020.04.287
[23] J. Zhang, J. Chen, Y. Zhang, S. An. J. All. Comp., **860**, 158473 (2021). DOI: 10.1016/j.jallcom.2020.158473
[24] M. Pollnau, D.R. Gamelin, S.R. Lüthi, H.U. Güdel, M.P. Hehlen. Phys. Rev. B, **61**, 3337 (2000). DOI: 10.1103/PhysRevB.61.3337
[25] W. Feng, X. Zhu, F. Li. NPG Asia Materials, **5** (e75), 63 (2013). DOI: 10.1038/am.2013.63

Translated by E.Potapova